Synthesis and Electrorheological Activity of a Modified Kaolinite/Carboxymethyl Starch Hybrid Nanocomposite

Xiaopeng Zhao, Baoxiang Wang, Jia Li

Institute of Electrorheological Technology, Department of Applied Physics 141, Northwestern Polytechnical University, Xi'an 710072, People's Republic of China

Received 8 June 2007; accepted 1 November 2007
DOI 10.1002/app.27742
Published online 25 February 2008 in Wiley InterScience (www.interscience.wiley.com).

ABSTRACT: According to physical and chemical designs, a novel modified kaolinite/carboxymethyl starch (CMS) nanocomposite was synthesized with a displacement method with dimethyl sulfoxide modified kaolinite as an intermediate. The material characterizations were carried out by X-ray diffraction, transmission electron microscopy, thermogravimetric analysis, and scanning electron microscopy. The analyses showed that kaolinite was dispersed at the nanometer-scale segments into the CMS matrix. The electrorheological behavior of the modified kaolinite/CMS hybrid nanocomposite dispersed in silicone oil was investigated. Under electric field strength (E) = 4 kV/mm and shear rate ($\dot{\gamma}$) = 105 s^{-1}, the shear stress of the modified kaolinite/CMS nanocomposite electrorheological fluid could be up to 8380 Pa, which was 10.4 times that of the electrorheological fluid at zero field. The modified kaolinite/CMS nanocomposite electrorheological fluid also exhibited good sedimentation properties. © 2008 Wiley Periodicals, Inc. J Appl Polym Sci 108: 2833–2839, 2008

Key words: clay; colloids; nanocomposites; nanotechnology; rheology

INTRODUCTION

In recent years, clay minerals have attracted great interest from researchers for the preparation and application of organic–inorganic nanocomposites.[1–4] Because of their small particle size and intercalation properties, they exhibit unexpected clay–polymer nanocomposite properties, especially for high-performance engineering materials with enhanced stiffness and strength, reduced permeability, and thermal and self-extinguishing characteristics. Clay–polymer nanocomposites have been reported with mainly montmorillonite but also recently with kaolinite.[5–9] Kaolinite is a 1 : 1 dioctahedral clay mineral with the ideal composition of $Al_2Si_2O_5(OH)_4$. Its structure is composed of $AlO_2(OH)_4$ octahedral sheets and SiO_4 tetrahedral sheets. The interlayer space of kaolinite is unsymmetrical, allowing particular reactions.[10–14] This asymmetry creates large superposed dipoles in the lamellar structure, which results in a large cohesive energy. Consequently, the intercalation chemistry of kaolinite is less developed than that of the swelling smectites.[15,16] Examples of kaolinite intercalation with small polar molecules, such as dimethyl sulfoxide (DMSO), potassium acetate, and, are frequently reported in the literature.[17–21] The intercalation of other compounds (especially polymer) with the aforementioned compounds as intercalated precursors is known as the *displacement method*.[15,16,22] However, as novel nanocomposites, the electrorheological (ER) behavior of kaolinite-based nanocomposites has rarely been studied.

Electrorheological fluid (ERF) typically consists of electrically polarizable particles dispersed in low-dielectric-constant oils. The application of an electric field can induce the polarization of the dispersed particles. As a result, a chainlike structure can be formed along the electric field direction in a few milliseconds, and the apparent viscosity can be enhanced greatly.[23–27] Because of their controllable viscosity and short response time, ERF materials are regarded as smart materials for active devices, brakes, clutches, shock absorbers, and actuators. Recently, they have expanded into some newly developed applications, such as human muscle stimulators, spacecraft deployment dampers, seismic controlling frame structures, ER tactile displays, and photonic crystals.[28–30] Previous studies on ERF materials have focused on inorganic oxides and organic polymers. Inorganic oxide ERF materials, such as

Correspondence to: X. Zhao (xpzhao@nwpu.edu.cn).
Contract grant sponsor: National Natural Science Foundation of China for Distinguished Young Scholars; contract grant number: 50025207.
Contract grant sponsor: National Natural Science Foundation of China; contract grant number: 50272054.
Contract grant sponsor: 863 Foundation; contract grant number: 2001AA327130.
Contract grant sponsor: Doctor's Foundation of the Ministry of Education of China.

titania, barium titanate, zeolite, gibbsite, saponite, hematite, and aluminosilicate, may have some shortcomings, which include high density, high friction, and poor antisedimentation properties.[31–35] Meanwhile, organic polymers, for example, polypyrrole, polyaniline, copolyaniline, poly(*p*-phenylene), β-cyclodextrin, and poly(acene quinine), also have some limitations, including toxicity and high cost.[36–39] A recent study of ERF materials focused on organic–inorganic composites, which could combine the advantages of two aforementioned materials.[40–44] To prepare high-performance organic–inorganic composite ER materials, a combination method of physical and chemical designs was adopted in our research group. Physically, the ER effect originates from the dielectric polarization of particles. The parameters, in connection with particle polarization, such as dielectric constant, dielectric loss, and conductivity, are considered a basic factor dominating the ER effect. It is well known that the chemical natures, including the molecular and crystal structures of materials, are critically important to the dielectric and polarization properties. Thus, it is possible for one to modify the dielectric and polarization properties by designing the molecular and crystal structure of the ER materials.[45,46] Clay minerals have attracted great interest in the field of organic/inorganic nanocomposites because of their small particle size and porous, lamellar, ion-exchange, and intercalation properties; their composites exhibit unexpected synergistic effects from the two components. A polyaniline/montmorillonite clay nanocomposite with an intercalated nanostructure has been used as ER material that not only possesses high yield stress but also has good antisedimentation and temperature abilities. This nanocomposite possesses an extended conductor polymer chain intercalated between the nanometer size interlayer, and the confinement of the clay gallery can also reduce the conductivity.[47,48] This is in accord with the dielectric design , which could be worthy for the preparation of other clay-based nanocomposite ERFs. Carboxymethyl starch (CMS), as opposed to starch, is a cold-water-soluble starch ether, which may be beneficial for the enhancement of the interaction with hydrophilic clay (kaolinite). Its polar organic groups, such as —OH and —COOK, can also be very helpful for enhancing the polarizability. Therefore, kaolinite and CMS were chosen for the preparation of a nanocomposite by a displacement method, which could improve its ER effect notably.

With a combination of physical and chemistry designs, modified kaolinite/CMS nanocomposites were prepared by means of the displacement method, and DMSO was used as an intermediate precursor. When the modified kaolinite/CMS nanocomposite was prepared, its ER properties were studied as a function of electric field strength, shear rate, and concentration.

EXPERIMENTAL

Materials

The kaolinite sample used in this study was from Shanghai, China. It was received as a finely divided white powder of high purity, and the phase composition of the kaolinite was examined by X-ray diffraction (XRD). The kaolinite was used without further purification. Corn starch was purchased from Tan Jin Chemical Third Co. (Tianjin, China). DMSO (Bei Jing Yatai Co., Beijing, China), potassium hydroxide (Xi'an Chemical Factory, Xi'an, China), and chloroacetic acid (Cheng Du Associated Chemical Institute, Chengdu, China) were used as received.

Synthesis of the modified kaolinite/CMS nanocomposite ERF

Preparation of CMS

First, the 20 g of cornstarch and 150 mL of ethanol were placed in a 500-mL vessel and stirred for 1 h. Then, sodium hydroxide (25 g) was added and reacted for 1 h at 30°C. After that, a mixture of 25 g of potassium hydroxide and 70 g of chloroacetic acid was added to the vessel and stirred for another 5 h at 50°C. The product was filtered and washed several times with ethanol and then dried *in vacuo* at 60°C. The resulting CMS was crushed in a mortar.

Preparation of DMSO-modified kaolinite

Kaolinite (10 g) was mixed with 180 mL of DMSO and 20 mL of distilled water and stirred at 80°C. After 24 h, the resulting material (kaolinite–DMSO) was filtered and dried in a vacuum oven at 80°C for 10 h to eliminate the DMSO adsorbing on the surface of the kaolinite.

Preparation of the modified kaolinite/CMS nanocomposite

In a 500-mL vessel, 10 g of the kaolinite–DMSO complex and 200 mL of distilled water were mixed and stirred at room temperature for 2 h. Then, 12 g of CMS was dissolved in 100 mL of distilled water and dripped into the vessel. After the dripping, the reaction temperature was increased to 80°C, and the mixture was violently stirred at 1500 rpm for 12 h. The product was filtered off and washed three times with ethanol and water, respectively, and then dried *in vacuo* at 60°C for 4 h and at 80°C for 2 h. The obtained modified kaolinite/CMS nanocomposite was then ground for 5 h in a ball mill and dried *in vacuo* at 80°C for 2 h.

Preparation of ERF

The silicone oil was first dried at 100°C for 2 h, and then, ERFs were prepared by dispersion of the nanocomposite particles (at different volume percentages) in silicone oil (dielectric constant (ε_f) = 2.60–2.80, conductivity (σ_f) = 10^{-12} to 10^{-13} S/m, density = 0.9–1.0 g/cm^3, viscosity = 500 mPa s, temperature = 25°C).

Characterization methods

Powder XRD patterns were obtained with a Rigaku diffractometer (D/III-γA, Tokyo, Japan) with Cu Kα radiation at a scanning rate of 1°/min. All measurements were taken with a generator voltage of 40 kV and a current of 20 mA. Transmission electron microscopy (TEM) experiments were performed using a Philips Tecnai G^2 20 microscope (Eindhoven, The Netherlands) operating at 200 kV. The samples were prepared by the deposition of a drop of the suspension onto a holey carbon grid. Morphological study was carried out in a JSM-5800 scanning electron microscope operating at 20 kV. With this aim, the composites and the pure kaolinite were suspended in acetone with manual stirring, deposited by casting directly in the copper sample holder, and dried at room temperature. After that, they were sputter-coated with a thin gold film to avoid charge build-ups because of their low conductivity. In addition, the particles were also pressed into cylinders (ϕ = 11.3 × 2.0 mm^2) under 12 MPa of pressure. Then, the disks were broken, and the fresh cross section was shown up. So the cross section was sputter-coated with a thin gold film for the morphological study. The thermal stabilities of pure kaolinite, pure CMS, and modified kaolinite/CMS particles were examined by thermogravimetric analysis (2950 TGA HR V5.3C) (TA Instruments, New Castle, DE) in a nitrogen atmosphere at a heating rate of 10°C/min and a flow rate of 60 mL/min. Alumina was used as a reference material. Particle size distribution was measured via a particle size analyzer (Master Sizer E, Malvern, UK).

The static shear stresses (τ's) of ERF were measured by a parallel plate force transducer (Xi'an, China). A rotary viscometer (NXS-11A, Chengdu, China; the gap between the outer cup and the inner bob was 2 mm) and a high-voltage direct-current (dc) power source (GYW-0/0, Beijing, China; 0–10 kV) were used to research the rheological properties of the ERF (shear rate range = 0–105 s^{-1}). The ERF was placed into the gap between the stationary cup and the rotating bob. The ERF was sheared by an applied mechanical torque until the particle chain structure was broken so that slipping occurred between the cup and the bob. Thereby, the shear rate was observed when the flow of the ERF started. The viscometer equipped with a temperature controller was used to measure the temperature dependence of τ (the thermal rate was ca. 1°C/min). The dielectric properties of the ERF were measured with an automatic inductance-capacitance-resistance meter (WK-LCR 4225, Beijing, China) at different frequencies (100 Hz, 1 kHz, and 10 kHz).

RESULTS AND DISCUSSION

Structural characterization

The XRD spectra of kaolinite [Fig. 1(a)], kaolinite–DMSO precursor [Fig. 1(b)], and modified kaolinite/CMS [Fig. 1(c)] are illustrated in Figure 1. Characteristic maxima of raw kaolinite were observed at 2θ = 12.6° (very intense, sharp, and narrow), which corresponded to the basal spacing of kaolinite (0.715 nm). After DMSO intercalation, as expected, we observed that the XRD pattern of the original kaolinite was dramatically modified. The peak at 2θ = 12.6° in the original kaolinite, assigned as the first basal peak, d_{001}, greatly shifted in the intercalates to small reflection angles (2θ = 7.96°) produced by the presence of intercalated DMSO (1.120 nm).[43] However, through the displacement of CMS, significant differences occurred [shown in Fig. 1(c)]. The peak at 2θ = 7.96° corresponding to the kaolinite–DMSO intercalate disappeared completely. Furthermore, as shown in Figure 1(c), when the displacement of CMS was produced, the characteristic diffraction peak (d_{001}) also decreased sharply in intensity. The diffraction pattern shown in Figure 1(c) showed that most kaolinite layers were delaminated, whereas some layers retained their basal spacing. These results show that the modified kaolinite/CMS nanocomposite was obtained because of the nanolayer of kaolinite dispersing into the polymer matrix of CMS.

Figure 2 shows the TEM images of the modified kaolinite/CMS nanocomposite. On the basis of the

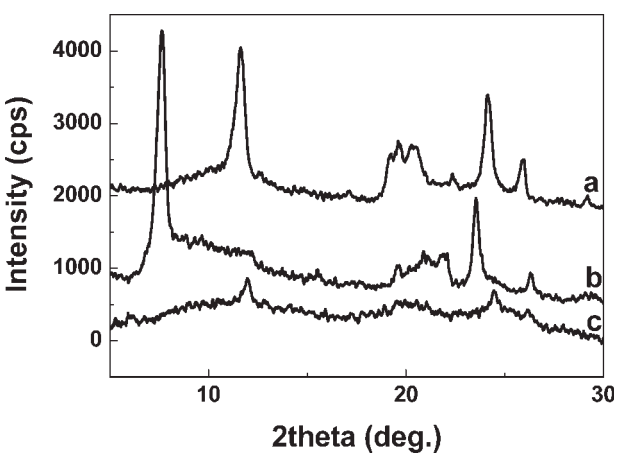

Figure 1 XRD patterns of (a) the raw kaolinite, (b) kaolinite–DMSO, and (c) modified kaolinite/CMS nanocomposite.

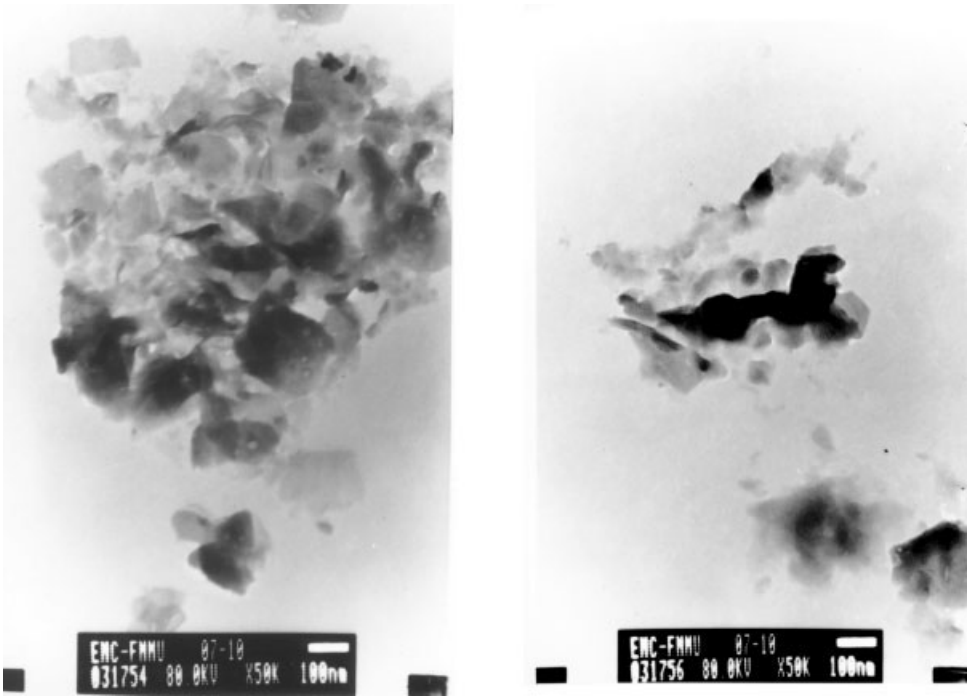

Figure 2 TEM images of the modified kaolinite/CMS nanocomposite.

analysis of the images, we determined that the dark irregular particles were the nanosegments of kaolinite, and the light area was CMS. The average kaolinite particle diameter of 30–100 nm for the kaolinite/CMS nanocomposite is shown in Figure 2.

The cross-section morphologies of pure kaolinite and the modified kaolinite/CMS nanocomposite are illustrated in Figure 3. As shown in the cross section of kaolinite [Fig. 3(a)], a stack of curly thin flakes for the kaolinite was distinctive. The thickness of the kaolinite layer was nanometer scale, and well-defined edges and corners could be seen. However, the cross section of the modified kaolinite/CMS nanocomposite showed that the stack disappeared, and the edge of kaolinite was unclear due to the coating of CMS.

Thermal analysis by thermogravimetric analysis is presented in Figure 4. The pure kaolinite showed two peaks at 49 and 496°C. These were attributed to the elimination of absorbed water and a dehydroxylation process in the kaolinite, respectively. The peak was

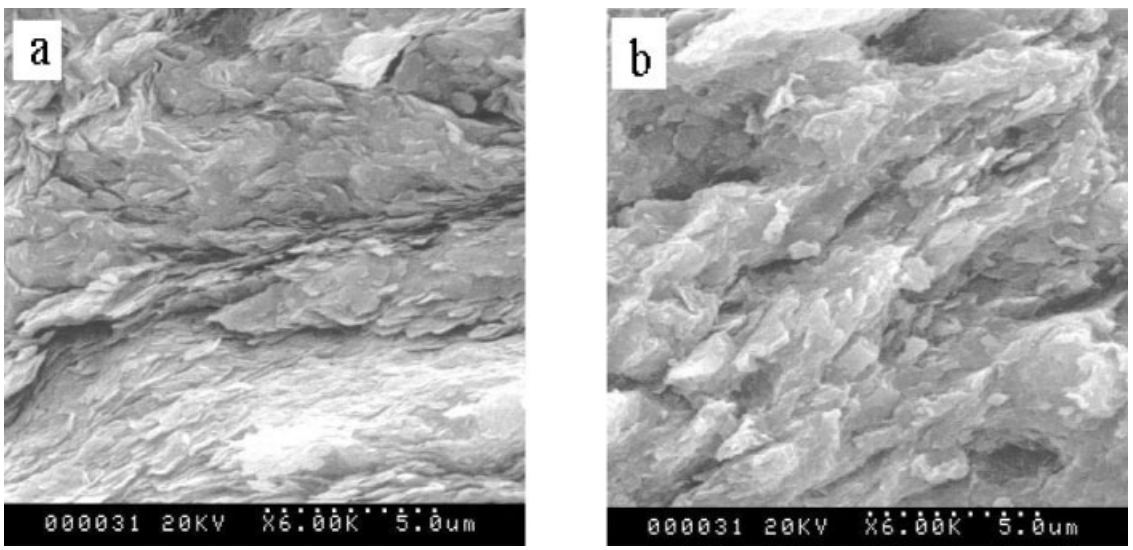

Figure 3 Scanning electron microscopy images of fresh cross sections of (a) the kaolinite and (b) modified kaolinite/CMS nanocomposite.

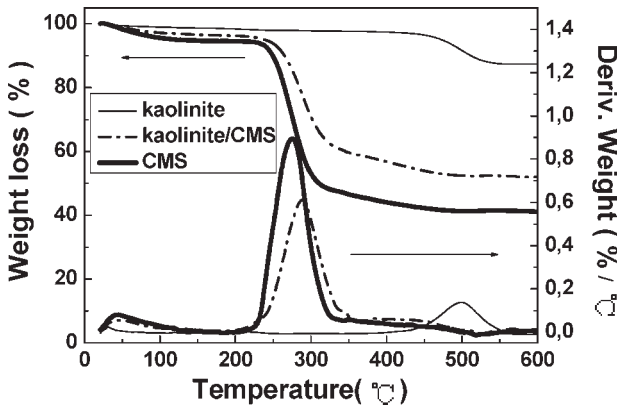

Figure 4 Thermogravimetric analysis/derivative thermogravimetry diagrams for kaolinite, CMS, and modified kaolinite/CMS particles.

visible in the CMS trace along with a strong peaks at 276°C corresponding to the carbonization and decomposition of CMS. However, the peaks in the modified kaolinite/CMS trace along with a strong peak moving to 288°C showed a better thermal stability than those of CMS. Furthermore, the peak of the dehydroxylation process of the kaolinite disappeared in the modified kaolinite/CMS trace, which may have been caused by the delamination of kaolinite. The weight loss of modified kaolinite/CMS around 100°C due to water or solvent used for washing was also lower than that of CMS. Thermal analysis by thermogravimetric analysis also provided the evidence of the kaolinite percentage in the nanohybrid. From room temperature to 600°C, the complete weight losses for pure kaolinite, pure CMS, and kaolinite/CMS nanocomposite particles were 12.7, 58.8, and 48.0%, respectively. So we obtained the kaolinite percentage in the nanohybrid with the following equation:

$$12.7\% \times \chi + 58.8\%(1 - \chi) = 48\%$$

where χ is the content of kaolinite is 23.5 wt %. This equation supposes that the weight loss of the composite is linear in comparison with a single constituent. From this, we deduced that the content of kaolinite in the nanohybrid was about 23.5 wt %. This value was slightly lower than the calculated value (29.41 wt %), which was obtained from the stoichiometric amount of raw materials.

Particle size distribution was measured via a particle size analyzer (Master Sizer E, Malvern). Figure 5 shows that the particle size (diameter) of the modified kaolinite/CMS was in the range 1–10 μm.

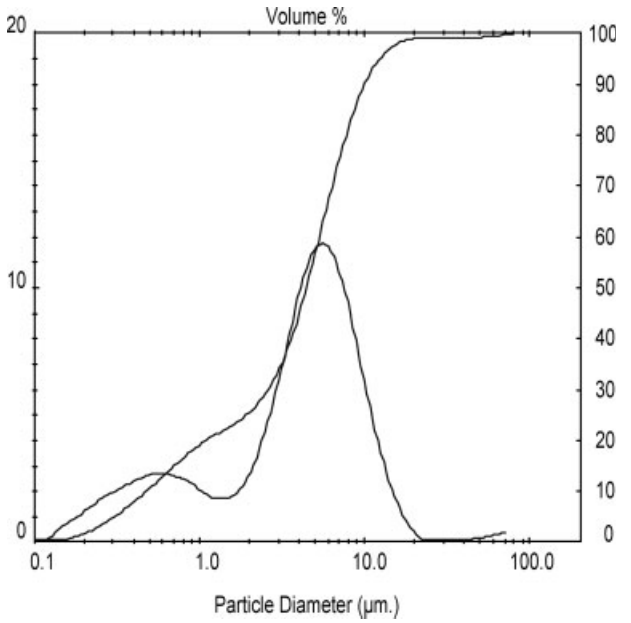

Figure 5 Particle size distribution of the modified kaolinite/CMS nanocomposite.

Rheological properties of the ERF

τ of the modified kaolinite/CMS ERF (31 ϕ %, where ϕ is the volume fraction) versus a change in the shear rate was measured under an applied electric field (ca. 0–4 kV/mm), and the results are plotted in Figure 6. The modified kaolinite/CMS nanocomposite ERFs under the electric field behaved as Bingham fluids immediately and showed high ER effects. Once the electric field was removed, they functioned as Newtonian fluids.[49–57] τ of the ERFs increased with increasing shear rate. Under conditions of 31 ϕ %, 25°C, electric field strength (E) = 4 kV/mm (dc), and $\dot{\gamma} = 105\ s^{-1}$, τ of the nanocomposite ERF was 8380 Pa. However, when the electric field was removed, τ was only near 800 Pa. The former was 10.4 times the latter, which showed that the modified

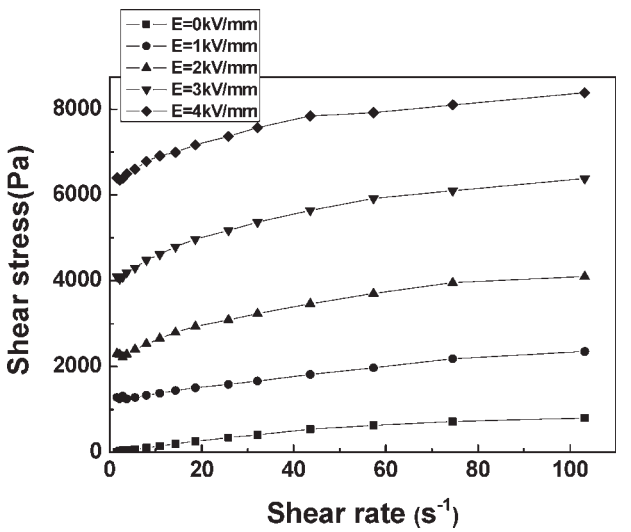

Figure 6 τ as a function of the shear rate for the modified kaolinite/CMS nanocomposite ERF under different electric fields.

kaolinite/CMS ERF demonstrated a significant ER effect. Bingham flow behavior, a suspension structure with a fibrillar or column structure, was observed. The fibrillar structure of particles assembled along with the applied electric field direction was destroyed via the imposed shear strain. τ depended on the particle interactions and the derivative of the electrostatic energy with respect to the shear strain. At the low shear rate region, the electrostatic interactions among particles (induced by the applied electric field) were dominant compared to the hydrodynamic interactions (induced by the external flow field). The fibrillar structures began to break and assemble repeatedly. The decrease in τ is also shown with an increase in shear rate at a low shear rate in Figure 6. That means, as the shear rate increased, the destruction rate of the fibrils became faster than the reformation rate. These phenomena were related to the rate of polarization under the shear by an applied electric field and was also observed for the ER materials.[40]

Figure 7 shows the τ values of the modified kaolinite/CMS nanocomposite with various values of ϕ (15, 20, and 31%) at 25°C under different electrical strengths. The bigger the volume percentage was, the higher the τ was that could be attained.

Figure 8 shows the static τ of modified kaolinite/CMS, kaolinite/DMSO, CMS, and pure kaolinite ERF with an increase in the dc electric field under a fixed shear rate (5 s^{-1}). As shown in the curves, τ of the modified kaolinite/CMS nanocomposite ERF was much higher than that of pure kaolinite ERF. The static τ of the modified kaolinite/CMS nanocomposite ERF was 4200 Pa under a 3-kV/mm dc field at 25°C and 31 ϕ %, with the leaking current density limited to 17 $\mu A/cm^2$. However, τ of the pure kaolinite ERFs was only 625 Pa, which was about 1/7 that of the nanocomposite ERF. Furthermore, τ of CMS ERF was close to 1000 Pa. These results show that the mechanical properties of the modified kaolinite/CMS nanocomposite were improved greatly because of the nanolayer of kaolinite dispersing into the polymer network of CMS, and the notable synergetic effect occurred. Moreover, the modified kaolinite/CMS composite was a two-dimensional scale nanocomposite; the interaction between the kaolinite layers and CMS chains may have enabled it to crosslink and form an entangled net. So the synergetic effect may have been caused by this crosslink to some degree.

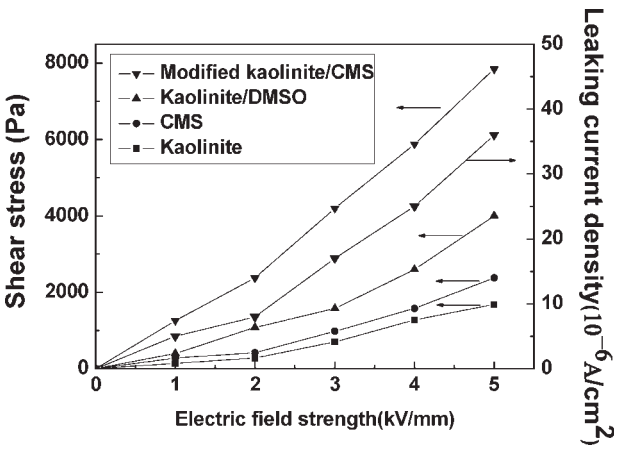

Figure 8 Static τ as a function of the dc electric field for modified kaolinite/CMS, kaolinite/DMSO, CMS, and kaolinite ERF (31 ϕ %).

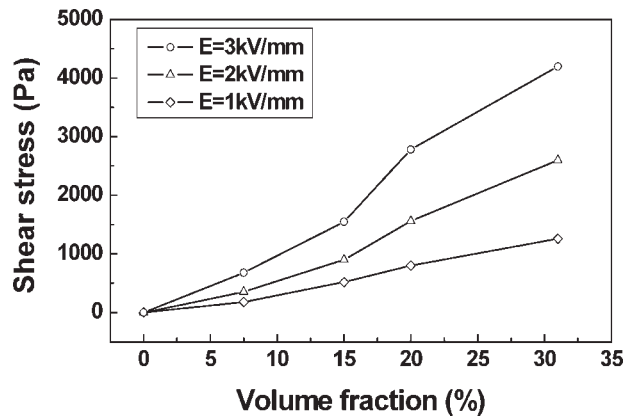

Figure 7 τ of the modified kaolinite/CMS nanocomposite versus the volume fraction under different electric strengths.

Sedimentation properties of the ERFs

The sedimentation properties of the ER materials are one of the main criteria used to evaluate whether the materials can be commercialized or not because the properties of ERF weaken rapidly along with the sedimentation of the particle phase. The general measure for enhancing the antisedimentation of ERF included control of the size of the particles, the preparation of

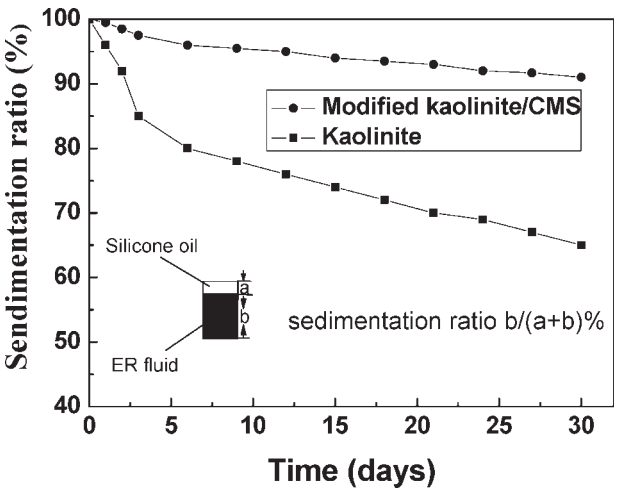

Figure 9 Sedimentation ratio of the modified kaolinite/CMS ERF and kaolinite ERF versus the time.

hollow or porous particles, the match of density between particles and oil, and the addition of the surfactant.[58] Because of its lamellar and open structure, kaolinite is a good suspension stabilizer. The density of the nanocomposite was decreased because of the existence of CMS. Moreover, the possible contact surface between kaolinite and CMS was increased because of exfoliation, so the sedimentation properties of the modified kaolinite/CMS nanocomposite ERF were improved greatly compared with those of pure kaolinite ERF. As shown in Figure 9, the sedimentation ratio of the modified kaolinite/CMS nanocomposite (15 ϕ %) ERF was 90% after 30 days, and its sedimentation stability increased notably more than the 67% of the pure kaolinite ERF.

CONCLUSIONS

A novel type of ER material, containing a modified kaolinite/CMS nanocomposite, was synthesized with a displacement method. The structure analyses showed that the nanoparticles of kaolinite were dispersed in the net of CMS. With the displacement of CMS, a stronger synergetic effect occurred, and the ER effect was optimized. The static τ of the modified kaolinite/CMS nanocomposite ERF was 4200 Pa under a 3-kV/mm dc field at 25°C and 31 ϕ %, with the leaking current density limited to 17 $\mu A/cm^2$. At the same time, τ of the pure kaolinite ERF was only 625 Pa, which was about 1/7 that of the nanocomposite ERF. The modified kaolinite/CMS nanocomposite ERF exhibited good sedimentation properties. All of these results exemplify a novel method for the preparation of ERF materials with good cost performance.

References

1. Rittigstein, P.; Priestley, R. D.; Broadbelt, L. J.; Torkelson, J. M. Nat Mater 2007, 6, 278.
2. Strawhecker, K. E.; Manias, E. Chem Mater 2003, 15, 844.
3. Kuila, B. K.; Nandi, A. K. Macromolecules 2004, 37, 8577.
4. Weimer, M. W.; Chen, H.; Giannelis, E. P.; Sogah, D. Y. J Am Chem Soc 1999, 121, 1615.
5. Gilman, J. W.; Jackson, C. L.; Morgan, A. B.; Harris, R.; Manias, E.; Giannelis, E. P.; Wuthenow, M.; Hilton, D.; Phillips, S. H. Chem Mater 2000, 12, 1866.
6. Vaia, R. A.; Jandt, K. D.; Kramer, E. J.; Giannelis, E. P. Chem Mater 1996, 8, 2628.
7. Letaief, S.; Detellier, C. J Mater Chem 2007, 17, 1476.
8. Itagaki, T.; Komori, Y.; Sugahara, Y.; Kuroda, K. J Mater Chem 2001, 11, 3291.
9. Frost, R. L.; Kristof, J.; Mako, E.; Martens, W. N. Langmuir 2002, 18, 6491.
10. Letaief, S.; Detellier, C. J Mater Chem 2005, 15, 4734.
11. Kristof, J.; Frost, R. L.; Martens, W. N.; Horvath, E. J Phys Chem B 2002, 106, 4162.
12. Kristof, J.; Frost, R. L.; Martens, W. N.; et al. Langmuir 2002, 18, 1244.
13. Horvath, E.; Kristof, J.; Frost, R. L.; Jakab, E.; Mako, T.; Vagvolgyi, V. J Colloid Interface Sci 2005, 289, 132.
14. Michaelian, K. H.; Lapides, I.; Lahav, N.; Yariv, S.; Brodsky, I. J Colloid Interface Sci 1998, 204, 389.
15. Tunney, J. J.; Detellier, C. Chem Mater 1993, 5, 747.
16. Letaief, S.; Detellier, C. J Mater Chem 2007, 17, 1476.
17. Michaelian, K. H.; Zhang, S. L.; Yariv, S.; Lapides, I. Appl Clay Sci 1998, 13, 233.
18. Frost, R. L.; Kristof, J.; Mako, E.; Kloprogge, J. Langmuir 1999, 15, 8787.
19. Takenawa, R.; Komori, Y.; Hayashi, S.; Kawamata, J.; Kuroda, K. Chem Mater 2001, 13, 3741.
20. Frost, R. L.; Kristof, J.; Kloprogge, J. T.; Horvath, E. Langmuir 2000, 16, 5402.
21. Komori, Y.; Enoto, H.; Takenawa, R. J.; Hayashi, S.; Sugahara, Y. S.; Kuroda, K. Langmuir 2000, 16, 5506.
22. Itagaki, T.; Kuroda, K. J Mater Chem 2003, 13, 1064.
23. Block, H.; Kelly, J. P. J Phys D: Appl Phys 1988, 21, 1661.
24. Halsay, T. C. Science 1992, 258, 761.
25. Wen, W. J.; Huang, X. X.; Yang, S. H.; Lu, K. Q.; Sheng, P. Nat Mater 2003, 2, 727.
26. Fossum, J. O.; Méheust, Y.; Parmar, K. P. S.; Knudsen, K. D.; Måløy, K. J.; Fonseca, D. M. Europhys Lett 2006, 74, 438.
27. Cao, J. G.; Huang, J. P.; Zhou, L. W. J Phys Chem B 2006, 110, 11635.
28. Hao, T. Adv Mater 2001, 13, 1847.
29. Wang, B. X.; Zhao, X. P. J Mater Chem 2002, 12, 1865.
30. Liu, L. Y.; Chen, X. Q.; Niu, X. Z.; Wen, W. J.; Sheng, P. Appl Phys Lett 2006, 89, 083505.
31. Filisko, F. E.; Radzilowski, L. H. J Rheol 1990, 34, 539.
32. Yin, J. B.; Zhao, X. P. Chem Mater 2002, 14, 4633.
33. Klingenberg, D. J.; Zukoski, C. F. Langmuir 1990, 6, 15.
34. Espin, M. J.; Delgado, A. V.; Plocharski, J. Langmuir 2005, 21, 4896.
35. Wang, B. X.; Zhao, X. P. Adv Funct Mater 2005, 15, 1815.
36. Wang, B. X.; Zhao, X. P. J Mater Chem 2003, 13, 2248.
37. Lengalova, A.; Pavlinek, V.; Saha, P.; Quadrat, O.; Kitano, T.; Steiskal, J. Eur Polym J 2003, 39, 641.
38. Cho, M. S.; Cho, Y. H.; Choi, H. J.; Jhon, M. S. Langmuir 2003, 19, 5875.
39. Quadrat, O.; Stejskal, J. J Ind Eng Chem 2006, 12, 352.
40. Sim, I. S.; Kim, J. W.; Choi, H. J.; Kim, C. A.; Jhon, M. S. Chem Mater 2001, 13, 1243.
41. Kim, J. W.; Liu, F.; Choi, H. J.; Hong, S. H.; Joo, J. Polymer 2003, 44, 289.
42. Jin, H. J.; Choi, H. J.; Yoon, S. H.; Myung, S. J.; Shim, S. E. Chem Mater 2005, 17, 4034.
43. Wang, B. X.; Zhao, X. P. J Solid State Chem 2006, 179, 1067.
44. Wang, B. X.; Zhao, X. P. J Mater Chem 2002, 12, 2869.
45. Wang, B. X.; Zhao, X. P. Langmuir 2005, 21, 6553.
46. Yin, J. B.; Zhao, X. P. Chem Mater 2004, 16, 321.
47. Kim, J. W.; Kim, S. G.; Choi, H. J.; Jhon, M. S. Macromol Rapid Commun 1999, 20, 450.
48. Zhao, X. P.; Yin, J. B. J Ind Eng Chem 2006, 12, 184.
49. Krzton-Maziopa, A.; Wycislik, H.; Plocharski, J. J Rheol 2005, 49, 1177.
50. Espin, M. J.; Delgado, A. V.; Gonzalez-Caballero, F. Phys Rev E 2006, 73, 041503.
51. Zhao, X. P.; Yin, J. B. Chem Mater 2002, 14, 2258.
52. Hong, C. H.; Choi, H. J.; Jhon, M. S. Chem Mater 2006, 18, 2771.
53. Parthasarathy, M.; Klingenberg, D. J Mater Sci Eng R 1996, 17, 57.
54. Pavlinek, V.; Saha, P.; Kitano, T.; Stejskal, J.; Quadrat, O. Phys A 2005, 353, 21.
55. Yin, J. B.; Zhao, X. P. J Phys Chem B 2006, 110, 12916.
56. Davis, L. C. J Appl Phys 1992, 72, 1334.
57. Block, H.; Kelly, J. P.; Qin, A.; Watson, T. Langmuir 1990, 6, 6.
58. Lu, J.; Zhao, X. P. J Colloid Interface Sci 2004, 273, 651.